The characteristics of the turbulence in the mixing region of a round jet

By P. O. A. L. DAVIES, M. J. FISHER AND M. J. BARRATT
Department of Aeronautics and Astronautics, University of Southampton

(Received 25 July 1962)

Measurements in the mixing region of a 1 in. diameter cold air jet are described for Mach numbers ranging from 0·2 to 0·55. The statistical characteristics of the turbulence in the first few diameters of the flow may be expressed in terms of simple kinematic similarity relationships. These are based on the jet diameter and the distance downstream from the jet orifice as length-scales, and the inverse of the local shear as a time-scale. The experiments show that the integral time scale of the turbulence in a frame convected with the maximum energy of the turbulent motion is inversely proportional to the local shear.

The most interesting result obtained is that the local intensity of the turbulence is equal to 0·2 times the shear velocity. This velocity is defined as the product of the local integral length-scale of the turbulence with the local shear. The local intensity is defined as the R.M.S. value of the local velocity fluctuations divided by the jet efflux velocity. It was found that the length-scale is proportional to the distance from the jet orifice, while the maximum shear is also related to this distance as well as to the jet efflux velocity. These two similarity relations break down close to the jet orifice and change beyond the first six or so diameters downstream. The convection velocity is not equal to the local mean velocity but varies slowly over the region of maximum shear when it is just over half the jet efflux velocity. The measurements of other observers fit the relationships obtained quite well. From these relationships it is possible to calculate the noise generated by the mixing region of a given jet directly, using expressions derived by Lilley (1958).

1. Introduction

The fundamental equations relating the noise produced by a jet to the turbulence in the highly sheared mixing region have been derived by Lighthill (1952, 1954) in his papers on sound generated aerodynamically. In the first paper he considers the exact equations of motion in a compressible fluid and compares these with the equations of sound propagation in a medium at rest. He shows that the exact equations may be written in the form

$$\frac{\partial^2 \rho}{\partial t^2} - a_0^2 \nabla^2 \rho = \frac{\partial^2}{\partial x_i \partial x_j}(T_{ij}), \tag{1.1}$$

where

$$T_{ij} = \rho v_i v_j + p_{ij} - a_0^2 \rho_0 \delta_{ij},$$

and v_i is the velocity component in the x_i direction, ρ the density, a_0 the velocity of sound in the fluid at rest and p_{ij} the compressive stress tensor. He also shows that at the low Mach numbers the dominant term in the stress tensor T_{ij} is $\rho v_i v_j$.

The momentum flux, $\int_V \rho v_i v_j dV$, can vary from point to point. But, for a given volume in the absence of solid boundaries the momentum ρv_i which is entering at one point must be balanced by momentum leaving elsewhere on the boundary. One therefore expects this mechanism to generate sound like two almost cancelling acoustic dipoles, that is like an acoustic quadrupole. Elements like T_{11} represent so called 'longitudinal' quadrupoles, and elements like T_{12} lateral quadrupoles.

Using the relationship that, for an observer at a distance $|X|$ large compared with the dimensions of the flow $|Y|$, the second space derivatives of T_{ij} can be replaced by second time derivatives. Lighthill shows that the solution to (1.1) becomes

$$\rho - \rho_0 \simeq \frac{x_i x_j}{4\pi a_0^4 x^3} \int_V \frac{\partial}{\partial t^2} T_{ij}\left(\mathbf{Y}, t - \frac{|\mathbf{X}-\mathbf{Y}|}{a_0}\right) dV(\mathbf{Y}), \tag{1.2}$$

where the integral is taken with retarded times so that only the sound from different parts of the volume V arriving at the same instant are added by the observer. In estimating this integral we know that, in a turbulent flow, velocity measurements at nearby points are well correlated but those at points more remote from each other are almost uncorrelated. We can therefore divide the turbulent flow into a number of regions such that the strengths of the quadrupoles within any one region are well correlated, but the strengths at points in different regions are uncorrelated (but see Lighthill 1954). Over a single group of correlated quadrupoles the pressure amplitude will add linearly while from uncorrelated quadrupoles only the R.M.S. amplitudes or energy intensities combine linearly. The extent of each independent quadrupole distribution can be taken as roughly the size of a typical energy-bearing eddy. For a typical frequency ω the ratio of eddy size to wavelength is $\omega l/a_0$, which tends to be small if the Mach number is small since ωl represents the amplitude of a typical velocity fluctuation. If this condition is satisfied it is usually possible to ignore variations in retarded time in distributions of non-zero total strength.

The above arguments all apply to the case where the Mach number is small. In a high-Mach-number flow Lighthill showed next that the sound radiated must be represented by moving quadrupoles convected at a speed U_c. The discussion is taken further in a later paper (Lighthill 1962). The radiation field relative to the position from which the sound is emitted by a moving quadrupole is expressed by

$$p - p_0 = x_i x_j \frac{\partial^2 T_{ij}}{\partial t^2}\left(t - \frac{r}{a_0}\right) \Big/ 4\pi r^3 (1 - M_c \cos\theta)^3, \tag{1.3}$$

where the function $T_{ij}(t)$ is the strength at time t, r is the distance from the observer to the point of emission, θ the angle between this direction and the direction of motion and M_c the convection velocity U_c divided by the speed of sound a_0. The effect of convection appears only in the $(1 - M_c \cos\theta)$ factors which

increase the sound emitted forwards somewhat more than they decrease that emitted backwards.

The overall intensity will be made up from the sum of the R.M.S. pressure components from each of the correlated source regions. Williams (1961) has shown that the total number of quadrupoles must be multiplied by $(1-M_c\cos\theta)$ to give that number whose radiation arrives simultaneously. The intensity from each quadrupole will contain a factor $(1-M_c\cos\theta)^{-6}$, and therefore the directional distribution of intensity will carry a factor $(1-M_c\cos\theta)^{-5}$ over and above that characteristic of the quadrupoles in the absence of convection.

In his second paper on the subject Lighthill (1954) considered the noise generated by the mixing region of a turbulent jet. Here he showed that turbulence of a given intensity could generate more sound in the presence of a large mean shear. He deduced that the dominant term in $\partial(\rho v_i v_j)/\partial t$ is the term

$$p(\partial v_i/\partial x_j + \partial v_j/\partial x_i) = pe_{ij}, \tag{1.4}$$

which means that we can use the substitution

$$\partial^2 T_{ij}/\partial t^2 \simeq (\partial p/\partial t)\,\bar{e}_{ij} \tag{1.5}$$

to estimate the sound generated by unit volume of turbulence. This relation, however, does not take us much further since there are no suitable techniques for measuring the velocity and pressure covariance directly to determine the distribution of $\partial^2 T_{ij}/\partial t^2$. This still awaits the development of experimental techniques for measuring static pressures directly.

Developing ideas put forward by Proudman (1952), Lilley (1958) showed how velocity correlations may be used to estimate the acoustic power output. These can be derived from measurements made with a hot-wire anemometer. Applying Lighthill's last result, (1.5), to the jet where the dominant rate of strain is $\bar{e}_{12}$ (corresponding to a velocity gradient $\partial\overline{U}/\partial x_2$) Lilley showed that the intensity per unit volume of turbulence is given approximately by

$$I(r) \simeq \{0{\cdot}02\sin^2\theta\cos^2\theta/\rho a_0^5 x^2(1-M_c\cos\theta)^5\}\,L_{11}^5\,\bar{e}_{12}^6\overline{\rho^2}\overline{v^2}\alpha, \tag{1.6}$$

where L_{11} is the longitudinal integral velocity scale of the turbulence and α is an anisotropy factor, probably of order 0·4. Thus it is seen that the noise output of a jet can be estimated if certain characteristics of the turbulence can be specified. Since it has not been possible to proceed far in this direction theoretically, these must be determined experimentally. The techniques for measuring these quantities are described in § 2 of this paper.

Many conclusions of the theory have already been verified experimentally, and some of the observed characteristics of jet noise are explained by Lighthill's theory. The high-frequency high-intensity sound is emitted mainly from the regions of the jet where the shear is high, and this is explained by the amplifying effect of shear. The observation that the sound is mainly radiated at an acute angle of the jet is explained by the radiation field pattern of convected quadrupoles. Finally, dimensional arguments based on the radiations from stationary turbulence show that the acoustic power output should vary as the eighth power of the jet velocity. This is close to the observed variation of peak intensity

and would at first sight confirm that agreement between theory and experiment is very good. However, as Lighthill (1962) and Curle (1961) have pointed out, this dependence is only achieved experimentally when the quadrupole convection effect is included. Thus, in a direction normal to the jet axis, where the convection effect is absent, exponents ranging from 5·5 to 7 are obtained in a large number of experiments (see Lilley & Westley 1952 and Gerrard 1956). It is suggested that this discrepancy may be due to a decrease in turbulence intensity at high subsonic Mach numbers, for which there is some experimental evidence.

Lilley (1958) has used the comprehensive turbulence measurements by Laurence (1956) to estimate the noise output of a jet and obtained fair agreement with the main experimental results. Laurence surveyed a cold subsonic jet for a distance of about 20 jet diameters downstream of the exit and presented measurements of the velocity profiles, turbulence intensities and spectra for a set of Mach numbers up to 0·7, the majority of the results being at 0·3. He also obtained the longitudinal and lateral velocity correlations and the single-point auto-correlations in a fixed reference frame for the whole region. He transformed the auto-correlation and compared this with the space correlation, and obtained good agreement in some instances. The results he reports are for a region for which the present investigation shows a frozen turbulence pattern to be a fair approximation. Others have used this result to obtain an estimate of the convection velocity appropriate to the analysis of the type discussed above.

This report describes similar measurements at the somewhat higher Mach number of 0·5, repeating Laurence's measurements of intensity and velocity distribution in more detail and including measurements with space separation and time delay to establish the convection characteristics more completely. The auto-correlations and spectra must be determined in terms of a frame of reference moving with the convection velocity U_c, which is defined as the apparent velocity of transport of optimum correlation. The turbulence characteristics required to define, for example, the integral scale L_{11} can be obtained from the space correlations. The majority of the measurements have been confined to the first few jet diameters where the shear is high and where most of the high-intensity noise originates. Single and pairs of hot wires have been used for all the velocity measurements and most of the results obtained from correlation of the hot-wire signals. Some of the experimental techniques have been developed at Southampton over the past seven years and are described in some detail in § 2 of the paper. The experimental results are given in § 3, where comparisons are made with previous work, while new results are discussed in § 4.

2. Experimental techniques

The experimental methods fall naturally into two groups, one being those employing single hot wires, and the other those with pairs of hot wires. Single hot wires can be used to measure the turbulence intensity, and the frequency spectra, either by using a narrow-band filter or transforming the auto-correlation. Pairs of hot wires can be used to define the size and shape of the regions in which the turbulent velocities are correlated. In addition measurements of space

correlations at retarded times can be used to define a convection velocity. It is then possible to obtain spectra and time scales in the frame moving with the turbulence. Before describing each of the above measurements in detail a brief description of the equipment is given, together with an estimate of the accuracy of the measurements. This is desirable because an understanding of the performance of the equipment plays a vital part in the interpretation of the measurements obtained.

2.1. *Measuring equipment*

The hot-wire anemometers used for the measurements were co-called constant-temperature instruments where the wire is kept at a constant resistance in a Wheatstone bridge circuit fed in closed loop by a high transconductance d.c.

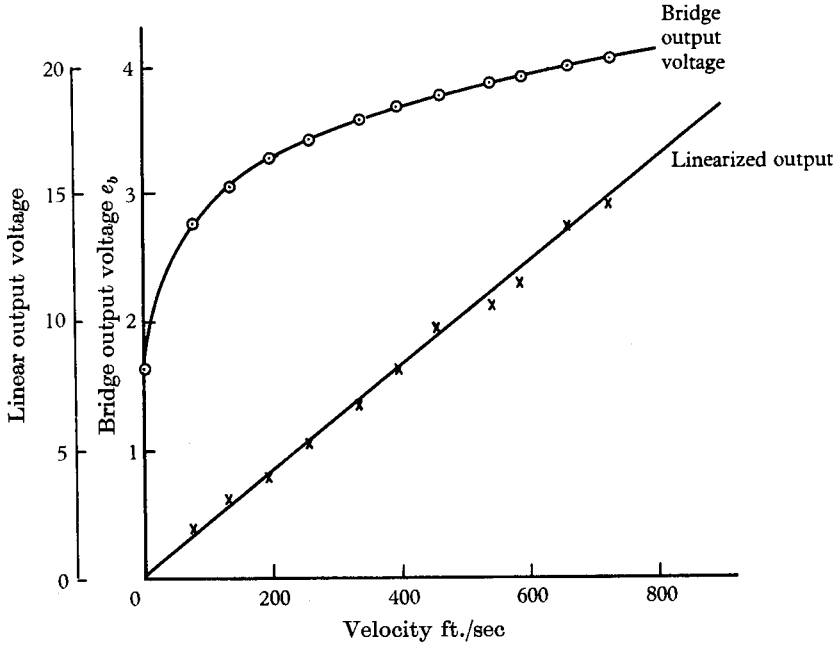

FIGURE 1. Calibration of hot-wire anemometer.

amplifier. The anemometer can be conveniently calibrated in any steady flow and the core of the jet one diameter from the orifice was used for this purpose. The output is non-linear but it was linearized by a function generator consisting of a chain of biased diodes and summing amplifiers. The chain was adjusted experimentally and the performance was quite good, as can be seen from figure 1.

A good approximation for the uncompensated system is

$$e \propto u^{\frac{1}{2}}, \quad 30\,\text{ft./sec} < u < 500\,\text{ft./sec},$$

where e is the voltage output and u the mean velocity. The hot-wire calibration fitted this relation to within $\pm 2\,\%$, while the actual calibration curve was repeated with many wires to an accuracy of $\pm 1\,\%$. The linearized signal gave

a similar repeatability of $\pm 1\%$ when small variations in wire cold-resistance had been balanced out on the bridge. The wires generally failed by being broken on impact by a small particle in the flow. They were, however, run at a temperture high enough to oxidize tungsten slowly which caused a rapid change of calibration just before they burned out. This did not occur until they had run many hours, and was not a frequent cause of failure. Measurements made just before a wire failure were always repeated.

The hot wires were made from 5 μ-diameter tungsten wire with the ends copper-plated leaving 2 mm bare at the middle. These were then soldered across the ends of fine-pointed conductors 4 mm apart to make a probe. Each probe was mounted on a separate micromanipulator, allowing independent adjustment of each wire. Wire position was adjusted to 0·1 mm, and reset to these limits using a pair of crossed telescopes as a fixed reference. This precision was essential as the jet was only 1 in. in diameter and the shear region near the jet orifice quite thin.

Careful measurements at Southampton have shown that the wire heat loss was not very sensitive to the relative flow direction over the range defined above. This is in good agreement with Sandborn & Laurence (1955). Both sets of results show that, with the airflow at 60° to the wire axis, the bridge voltage was only reduced by 3% compared with that for flow normal to the wire at the higher velocity, and by 5% at the lower velocity stated above. With the flow parallel to the wire axis, the signal was reduced by 30% compared with the normal setting. These results indicate that the bridge output depends partly on the velocity components along the wire and not only on the normal component as has often been assumed.

Further experiments indicated that heat conduction to the supports represented a substantial proportion of the heat loss from the wire, giving rise to a temperature gradient along the wire. Any substantial velocity component along the wire modifies the temperature gradient considerably, the overall effect being to increase the end loss. This effect for a wire of given dimensions will be much more serious for tungsten wires which have a much higher thermal conductivity than for platinum ones. This can be seen by comparing the results given above with those reported for platinum wires by Webster (1962). The interpretation of hot-wire measurements must therefore be made with some care. For practical purposes, however, an anemometer with its axis normal to the mean velocity, provided the mean flow is greater than two or three times the larger velocity fluctuations, will respond to the magnitude of the instantaneous velocity and not to its direction.

The frequency response of the hot-wire amplifier was flat (within 1 db) from d.c. to 80 kc/s while the linearizer had a response that was flat (within 0·2 db) from d.c. to 10 kc/s. As the observed turbulence frequency spectra level at 10 kc/s was -20 db relative to 1 kc/s it was assumed that the bridge voltage followed the flow velocity with similar phase shift and attenuation for both wires during the correlation measurements.

The mean voltage was measured with a carefully calibrated voltmeter. A true R.M.S. voltmeter was used for intensity measurements (a.c. component only) and a twin-channel tape-recorder for the correlation measurements. Tests showed that

a 10 sec integration time on the correlator gave a reasonably small scatter above 100 cycles, while the two tape-recorder channels were well matched within a correlation count of $\pm 0{\cdot}02$ when checked between 150 c/s and 8 kc/s with white noise. The correlator which has been described in detail elsewhere (Allcock, Tanner & McLachlan 1962) gives a similar performance (correct within $\pm 0{\cdot}02$) from d.c. to 10 kc/s provided the background noise level is low. Time delays between correlator channels were provided up to 140 msec in 2 μsec steps. Provided proper care was taken, it was found that simple measurements could be repeated to within 2 % or a correlation count of 0·02, although a larger scatter on correlation results was observed occasionally. This could usually be traced to a rise in the relative noise-to-signal ratio on the tape.

2.2. *Single-wire measurements*

Single wires were used to measure mean velocity, turbulence intensity, spectra and fixed-point auto-correlations. The spectra and auto-correlations represent a velocity pattern being convected past the fixed hot wire. Laurence (1956) discussed the conversion of these measurements to true moving-frame spectra at some length but there are certain difficulties in doing this as will be seen later. The chief effect in these experiments is that the high convection velocity increases the bandwidth requirements of the equipment. The moving-frame spectra can be obtained by other methods which are discussed later (see § 2.3).

Mean velocity measurements. Calibration of the hot wires showed that the bridge output voltage represented some function of the instantaneous velocity magnitude $|u|$, and was for practical purposes independent of the flow direction provided the wire had its axis normal to the mean velocity vector, U. If the fluctuating velocity components are v_1, v_2, v_3, then

$$|u| = [(U+v_1)^2+v_2^2+v_3^2]^{\frac{1}{2}} \simeq U\left[1+\frac{v_1}{U}+\frac{v_2^2+v_3^2}{2U^2}\right],$$

ignoring higher powers of the fluctuations than the second. If the hot-wire system has a linear response so the output voltage e is proportional to $|u|$, then the mean voltage $\bar{e}$ represents the velocity given by

$$\bar{e} = k_1 U[1+\overline{\delta^2}], \tag{2.1}$$

where δ is of the order v/U, and over bars represent time-mean values. The instantaneous voltage fed to an R.M.S. meter or tape-recorder with the d.c. component removed is therefore

$$e-\bar{e} = k_1 U[(v_1/U)+(\delta^2-\overline{\delta^2})] \simeq k_1 v_1, \tag{2.2}$$

which defines the resultant turbulent signal with an error of 2 % if the three components of the turbulence have intensities I equal to 0·2; where U_0 is the jet velocity,

$$I = (\overline{v^2})^{\frac{1}{2}}/U_0 \tag{2.3}$$

is a convenient definition of turbulence intensity.

For the non-linear hot wire, the relation between actual bridge volts e_b and velocity $|u|$ was found to be approximated by

$$e_n = e_b - e_a = k_2 |u|^{\frac{1}{4}} \simeq k_2 U^{\frac{1}{4}} \left[1 + \frac{v_1}{4U} + \frac{\delta^2}{8}\right], \tag{2.4}$$

where e_a is the bridge voltage for zero velocity, see figure 1, and $\bar{e}_n \simeq k_2 U^{\frac{1}{4}}$ to a better approximation than for the linear wire. The hot-wire signal output then becomes, when recorded on tape,

$$e_n - \bar{e}_n = \tfrac{1}{4} k_2 U^{-\frac{3}{4}} v_1, \tag{2.5}$$

which involves a more detailed calibration to estimate v_1 accurately than with a linear hot-wire system.

Turbulence intensity. For a linear system, the intensity can be obtained directly. Defining the R.M.S. signal

$$(\overline{e_1^2})^{\frac{1}{2}} = \{\overline{(e-\bar{e})^2}\}^{\frac{1}{2}} = k_1 U[(\overline{v_1^2}/U^2) + \overline{\delta^4 - 2\delta^2\bar{\delta}^2 + (\bar{\delta}^2)^2}]^{\frac{1}{2}}$$

and ignoring the terms in δ^4 which must be nearly zero, this gives

$$I_l = (\overline{e_1^2})^{\frac{1}{2}}/\bar{e}. \tag{2.6}$$

Similarly for the non-linear anemometer,

$$I_n \simeq 4\{\overline{(e_n - \bar{e}_n)^2}\}^{\frac{1}{2}}/\overline{e_n}. \tag{2.7}$$

We also note that the average axial component intensity I can be obtained as

$$I = [\tfrac{8}{3}\{U(\bar{e}) - U(\overline{e_n})\}/U]^{\frac{1}{2}}.$$

However, the method is hardly an accurate one as it involves a small difference in large magnitudes.

Turbulence spectra. The recorded turbulence signal given by either of equations (2.2) or (2.5) can be analysed by a narrow-band frequency analyser to give the turbulence spectrum. The auto-correlation of the signal can be defined as

$$R_\tau = \frac{1}{T}\int_0^T \frac{\overline{v_1(0)\, v_1(\tau)}}{\overline{v_1^2}}\, d\tau, \tag{2.8}$$

where T is the integration time of the correlator, τ the time delay and v_1 being regarded as a function of time only. Usually, the signal levels on the two channels in the correlator may differ slightly, and if these are denoted by v_a and v_b, then

$$\overline{v_1(0)\, v_1(\tau)}/\overline{v_1^2} \equiv \overline{v_a v_b}/(\overline{v_a^2 v_b^2})^{\frac{1}{2}},$$

and although it will not be restated explicitly this process is generally implied when describing correlation coefficients.

The spectral density function $F(n)$ may also be determined from the Fourier transform of R_τ, namely

$$F(n) = 4\int_0^\infty R_\tau \cos 2\pi n\tau\, d\tau. \tag{2.9}$$

This method is more laborious experimentally than the former one, but can be used to obtain spectral density in a moving frame, provided R_τ is specified in this frame of reference. This was determined experimentally as detailed later (§ 2.3), and requires two-wire measurements.

Lateral component of mean velocity. Throughout the experiments, it has been assumed that the mean velocity direction is predominantly axial. As a check on this the lateral mean velocity V was estimated from the rate of change in the streamwise direction of the radial distribution of axial velocity. Using the axial

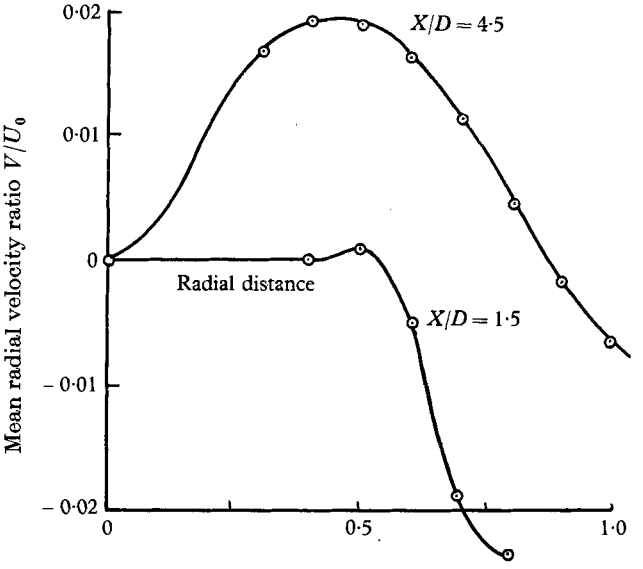

FIGURE 2. Radial component of mean velocity.

symmetry of the jet, the equation of continuity of mean flow can be integrated to give

$$V(r) = -\frac{1}{r}\int_0^r \left[r_1 \frac{\partial U}{\partial x_1}\right] dr,$$

where $\partial U/\partial x_1$ is estimated at each radius r_1. The estimated values of V have been plotted against distance from the axis, Y/D, where D is the jet diameter. The velocities are rendered non-dimensionless by dividing by the core velocity U_0. These results are plotted on figure 2 for two distances X/D from the jet orifice. As can be seen, the assumption that the mean velocity is axial is reasonable except at the outer edge of the mixing region. In this part of the flow, equations (2.2) to (2.7) will become unreliable. It has been shown in the Introduction that this region is unlikely to contribute a large portion of the total noise output as the shear is small, so it has not been included in the detailed experiments.

2.3. *Two-wire measurements*

Two-wire measurements can be used to define the length-scales of the turbulent velocity fluctuations and the auto-correlation in a moving frame. As seen from

equation (2.2) the correlations will always refer to the fluctuating velocities in the mean flow direction, which is taken to be along the jet axis.

Space correlations and space scales. The signals from two hot wires separated by a distance x can be correlated to define the region over which the velocities at the two points are strongly related. These results can then be used to define a typical 'eddy' size, or the integral length-scale L_x. The axial-velocity space correlation coefficient is defined as

$$R_{x_1} = \frac{1}{T}\int_0^T \frac{\overline{v_1(0)\,v_1(x)}}{\overline{v_1^2}}\,dt \tag{2.10}$$

with similar definitions for displacements in other directions. Here $v_1(0)$ and $v_1(x)$ are each regarded as functions of time. The space-scale L_{x_1} can be defined by

$$L_{x_1} = \int_0^\infty R_{x_1}\,dx, \tag{2.11}$$

which can be related to the turbulence scale L_{11} of equation (1.6) provided the three components of the space correlation are known.

Cross-correlation. If the signal from one of the two wires is also delayed a time τ before being correlated with the other, then correlations with a space separation and time delay are obtained. The cross-correlation is therefore defined as

$$R_{x\tau} = \frac{1}{T}\int_0^T \frac{\overline{v_1(0,0)\,v_1(x,\tau)}}{\overline{v_1^2}}\,dt. \tag{2.12}$$

If the values of $R_{x\tau}$ are plotted against time delay for a series of increasing wire separations the whole family of curves define an optimum correlation envelope in time. The convection velocity of the energy-bearing eddies can be found by measuring the time delay at which each wire-separation curve touches the envelope. The ratio of wire separation to this time delay then defines the convection velocity for this separation. The envelope is also the auto-correlation of the energy-containing eddies $R_{\tau c}$ in a reference frame moving with the convection velocity U_c. The moving-axis integral time-scale, which defines the rate at which the turbulence pattern changes in time, is then

$$L_\tau = \int_0^\infty R_{\tau c}\,d\tau. \tag{2.13}$$

Alternatively an estimate of the time-scale may be obtained by fitting an exponential function to the correlation curve as discussed in detail by Laurence (1956). This is helpful when $R_{\tau c}$ does not reach zero within the range of the experiments. In this case the time-scale becomes

$$L'_\tau = \tau[R_{\tau c} = 1/e] \tag{2.14}$$

and similarly

$$L'_x = x[R_x = 1/e]. \tag{2.15}$$

These estimates were used later to define the ratio of time- to length-scales. If this ratio is large it implies that the turbulence may be regarded as a fixed pattern moving at the convection velocity. This gives a simplified description

of the turbulence that was first proposed by Taylor (1935). An alternative method of finding the convection velocity U_c is to plot isocorrelation contours of $R_{x\tau}$ on the (x, τ)-plane. These will be skewed at an angle to the τ-axis and the tangent of this angle will again define the convection velocity. The Fourier transform of the cross-correlation envelope will give the turbulence spectrum function in the moving frame. This can then be related to the spectrum of the noise field of the jet.

3. Experimental results

The aim of the experiment was to determine the distribution of shear, length scales, turbulence intensity and the convection velocity throughout the jet. There are nine components of the length-scale and three intensity components, but the present series of experiments has been restricted to the measurement of the axial scale and the intensity of the axial fluctuations. It is clear that measurements of all components are required for a complete statistical description of the turbulence structure, but it seems reasonable to assume that the components are all related. Laurence's measurements indicate that the axial components are the largest ones.

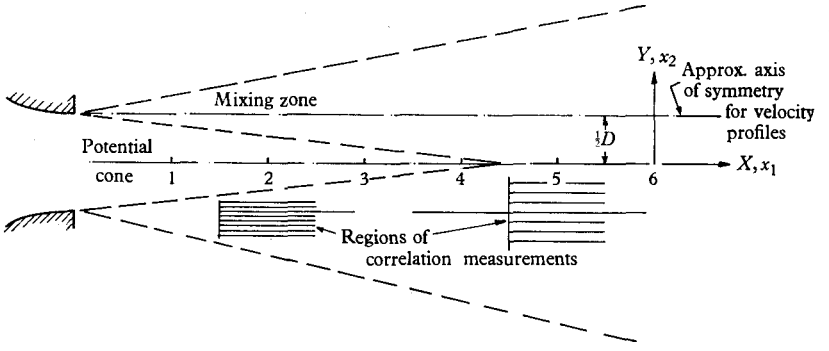

FIGURE 3. Jet flow geometry.

The general structure of a circular jet is well known and when the density of the jet is the same as that of the surroundings is similar for all jets (Townsend 1956). As shown on figure 3, a mixing zone of intense turbulence surrounds a cone of potential flow, which extends for about 4 diameters from the jet outlet. In the potential cone the mean velocity is equal to the jet exit velocity U_0. The turbulence intensity at the jet axis rises steadily from a very low value at the orifice but has reached one-quarter of the maximum intensity by 3 diameters downstream. At large distances from the orifice, the intensity is uniform across the middle half of the jet and then falls steadily to the boundaries (Townsend 1956). The mixing zone boundaries spread at a constant angle, and the jet continues to spread at a constant angle for very great distances from the orifice. The edges of the jet are not smooth but covered by a random distribution of relatively large discrete eddies which appear to increase in scale downstream with the general increase in jet dimensions. It has been well established that the jet diameter is the scale parameter for similarity of jet geometry.

Some of the measurements of length-scale, shear and intensity repeat the

measurements obtained by Laurence in a larger jet ($3\frac{1}{2}$ in. diameter) at a Mach number of 0·3, and confirm the kinematic similarity of the jet flow for the first few diameters even to details of the turbulence.

3.1. *Mean velocity and shear measurements*

The distribution of mean shear was estimated from mean velocity profiles measured throughout the jet. Although the mean velocity appears to be a relatively simple quantity to measure, to do so accurately is difficult, being subject to the errors indicated by equation (2.1). Measurements of the velocity profile with a Pitot tube are also subject to errors. One of these, the displacement of

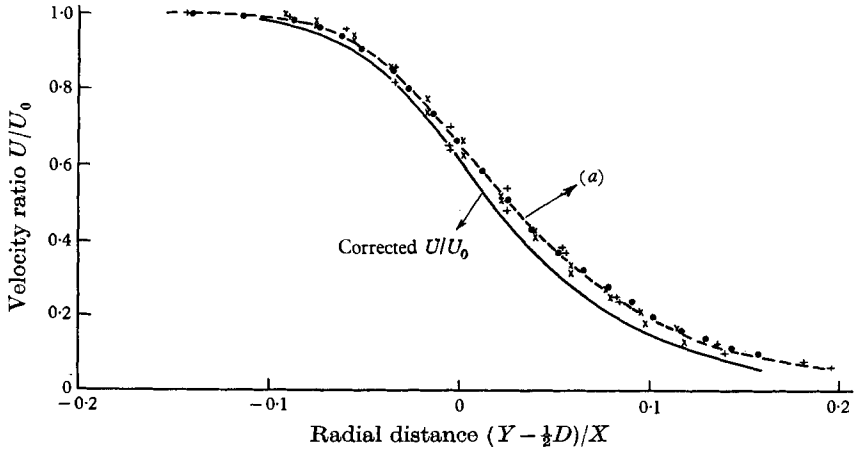

FIGURE 4. Mean velocity distribution in mixing zone. Distance from orifice, X (in.): +, 1·5; ×, 4·5; ●, 3·0. M_0: +, 0·27; ×, 0·45; ●, 0·30. $(a) = \dfrac{\bar{\varepsilon}}{e_0} \simeq \dfrac{\overline{U}}{U_0} + \left(\dfrac{v_1^2}{U_0^2}\right)^{\frac{1}{2}} \dfrac{U_0}{U}$.

the effective Pitot centre due to shear, can be estimated (Davies 1957) while errors due to the yaw sensitivity of the Pitot cannot, at least according to present knowledge. For this reason hot-wire measurements are likely to be as accurate as those with a Pitot, and perhaps better where both shear and turbulent intensity are high. However, check readings were made with a total-head tube giving results which seemed to agree with the hot-wire measurements quite satisfactorily.

Both linearized and non-linearized hot-wire anemometers were used to determine velocity profiles, the results differing slightly in the manner predicted above (§ 2.2), the largest difference being near the radial position $Y/D = 0{\cdot}4$. Mean dimensionless profiles measured at 1·5, 3 and 4·5 in. downstream of the orifice for two Mach numbers are plotted on figure 4. This illustrates the sort of scatter that can be expected from individual measurements, which tends to conceal any variation with Mach number. The corrected profile, taken from the results at 3 in. is also included on figure 4. This indicates the order of the errors in the velocity measurements due to the characteristics of the hot-wire anemometer which have been discussed previously. The corrections required seem small but modify the shear distribution significantly as can be seen from figure 5, where the gradient of the two profiles is plotted.

Careful analysis of all the results from velocity profile measurements also indicates some variation of shear with Mach number, though this has not been determined exactly, but it seems that, for example, doubling the Mach number does not quite double the shear. The same tendency can be seen in Laurence's

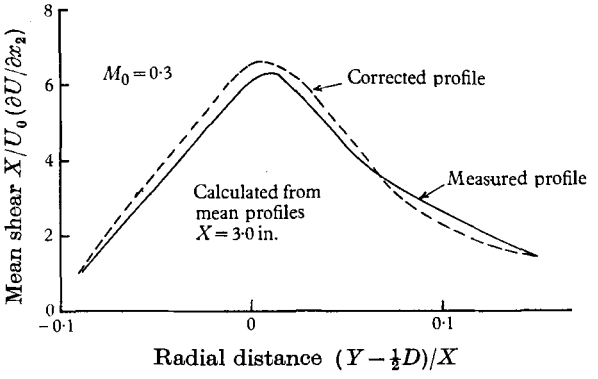

FIGURE 5. Radial distribution of mean shear.

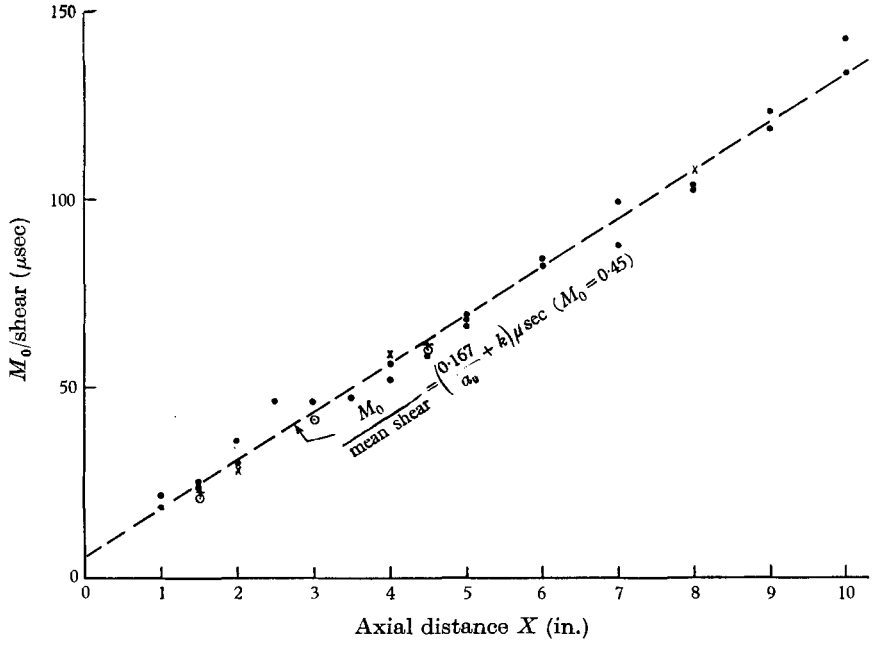

FIGURE 6. Maximum mean shear distribution (inverse plot). ●, 1·0 in. jet ($M_0 = 0{\cdot}45$). ×, Laurence 3·5 in. jet ($M_0 = 0{\cdot}5$). +, Figure 4 ($M_0 = 0{\cdot}45$). ⊙, Figure 4 ($M_0 = 0{\cdot}3$).

measurements for velocity profiles in the range $0{\cdot}2 < M_0 < 0{\cdot}7$ with a 3·5 in. diameter jet.

Estimates of the maximum shear have been obtained for the first 10 diameters of the jet flow, and are plotted on figure 6. To simplify the presentation, the inverse shear has been plotted as this yields an almost linear relationship and, furthermore, the improvement in accuracy as the width of the velocity profile

increases is reflected in the method of presentation. The scatter of the main results obtained at $M_0 = 0{\cdot}45$ is considerable and illustrates the difficulty of making accurate shear measurements, but the results appear to follow the general trend of a straight line. Laurence's results for a larger jet are also included together with estimates from the results presented in figure 4. For the majority of the results, a good fit to the measurements is given by the relation

$$(\partial U/\partial x_2)_{\max} = 6U_0/(X + ka_0)\sec^{-1} \quad (M_0 = 0{\cdot}45),$$

where k will depend on the thickness of the boundary layer in the flow leaving the jet nozzle. For the 1 in. jet, when $M_0 = 0{\cdot}45$, ka_0 was found to be 0·4 in., indicating an origin about 0·4 in. upstream from the orifice.

The remainder of the experimental work, with the exception of the turbulent intensity measurements, was concentrated in the region of high shear. Correlation measurements were made over radial planes $1\frac{1}{2}$ and $4\frac{1}{2}$ diameters from the jet orifice as this is where the high intensity noise originates (Lilley 1958 and Ribner 1958).

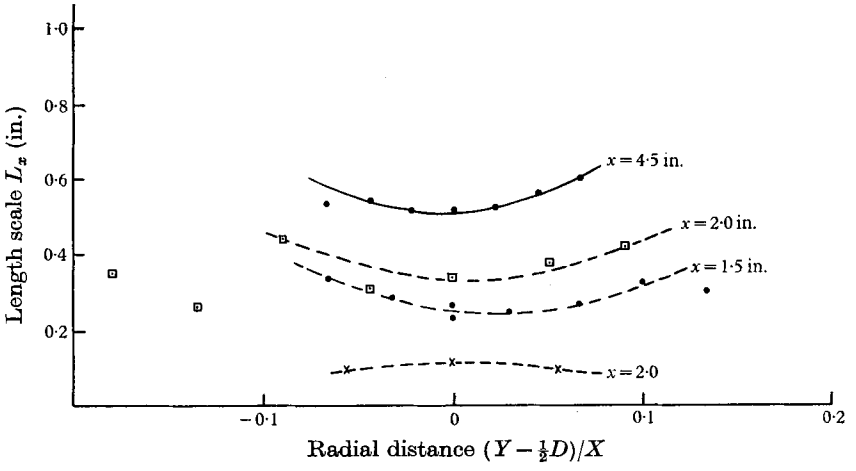

FIGURE 7. Radial variation of length scales in a jet.
⊡, Axial scale—Laurence. ×, Radial scale—Laurence.

3.2. *Space correlations and space scale measurements*

Space correlations were measured with the linearized equipment, and their general form was found to be in close agreement with Laurence's results, so they will not be illustrated here. The region of the jet surveyed in these measurements is shown in figure 3. For the majority of readings one wire was fixed at $1{\cdot}5D$ or $4{\cdot}5D$ from the jet orifice and the second wire traversed downstream from the fixed one. The moving wire was also traversed upstream, as a check, giving similar results, so this was not repeated at every fixed wire position.

The space correlations have been integrated in accordance with equation (2.11), to give the space-scales. The radial distribution of space-scales is shown on figure 7, which shows that the variation in axial scale is of the order of 20% across the mixing region. Axial scale estimates and similar results by Howard (1959) at Southampton and the two-wire results obtained by Laurence are also

plotted on figure 8 for comparison. In a few instances the R_x *vs* x curve went slightly negative. In calculating the length-scales only that part of the curve up to the first zero crossing was considered, as this gives a consistent definition of eddy scale. For this definition a fair fit to the results is given by $L_{x_1} = 0{\cdot}13X$ $(D < X < 6D)$. Provided the results are compared on the basis of distance from the jet orifice and the difference of jet size is ignored, the measurements agree very well. This is quite reasonable if one remembers that the thickness of the shear layer is not large compared with the dimensions of the jet, and that its thickness increases with axial distance downstream. The results also show that the scales of the turbulence increase almost linearly with axial distance and in the same way as the general dimensions of the shear layer. This is good evidence for the strong similarity of the mixing-region flow.

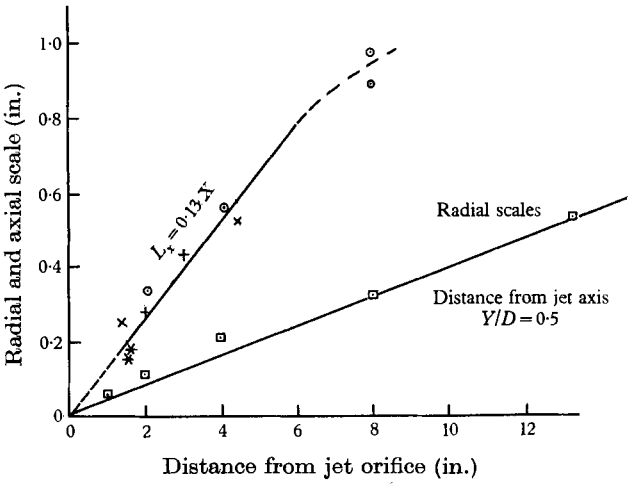

FIGURE 8. Axial and radial scales of axial velocity fluctuations. Longitudinal scales: ⊡, ⊙, Laurence (two wires); ×, $M_0 = 0{\cdot}45$; +, $M_0 = 0{\cdot}3$ (Howard); *, $M_0 = 0{\cdot}22$, $0{\cdot}45$.

Laurence's two-wire estimates of the lateral scale are also included for comparison on figure 8. The ratio of these scales in the mixing region is of the order 3 : 1 axial to radial. The radial eddy scale from his measurements is roughly one-quarter of the width of the shear layer defined from the intensity measurements. One can explain this difference in length-scales by considering the turtulence in terms of vorticity components, one radial, one axial and one tangential. The mean tangential filaments represent the mean shear, and radial filaments will be the ones strongly stretched by the shear. This implies a feed of energy into rotations about radial axes, so one could expect the longitudinal and tangential velocity fluctuations and scales to be larger than the radial ones. The results of Laurence were at $M = 0{\cdot}3$, while the present results were obtained at $M = 0{\cdot}45$. Checks were also made at $M = 0{\cdot}22$, and all the results give similar axial scales. This implies that the space-scale is independent of velocity and depends only on the position in the mixing region.

3.3. *Frequency spectra*

The turbulence signal from a hot wire can be analysed by a narrow-band frequency analyser to give the apparent turbulence spectrum. The frequency spectra obtained with 3rd octave filters at successive radial positions are plotted on figure 9. The results at 1·5 in. show a small change with radial position, but a systematic decrease in frequency with increase of radius is more obvious in those at 4·5 in. The change of bandwidth is, however, much less than would be expected

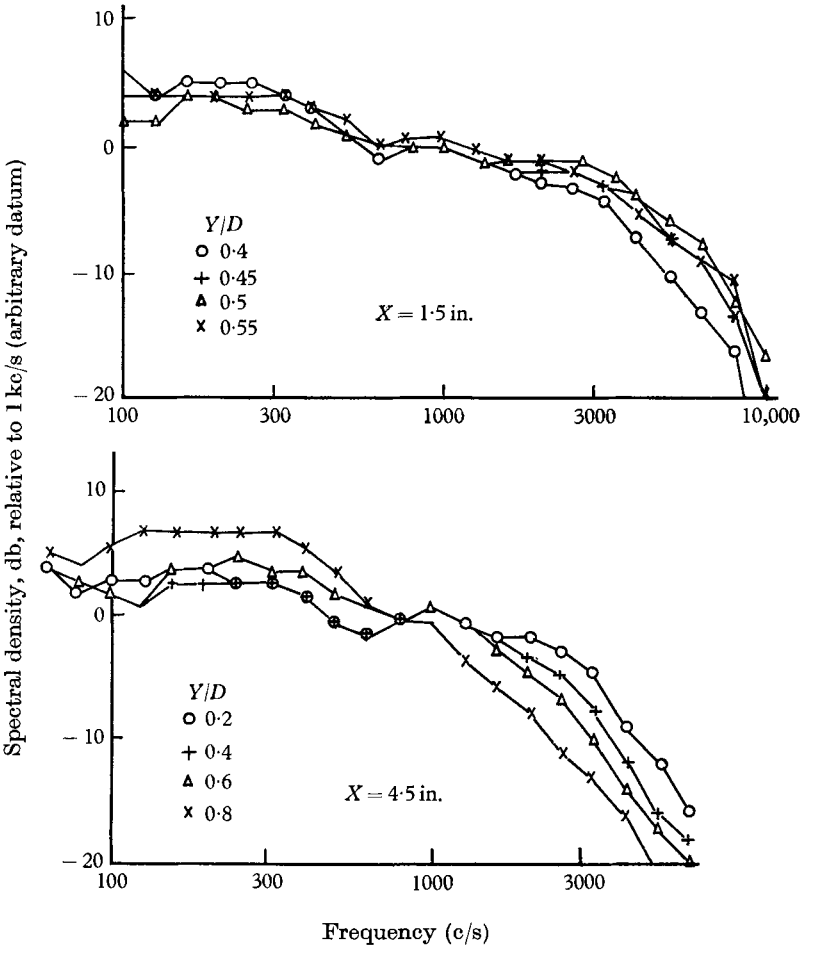

FIGURE 9. Spectral distribution of hot-wire signal.

if the eddy pattern described in the previous section were to be swept past the fixed hot wire at the local mean velocity. Alternatively, the eddy scale must decrease quite rapidly with radius which is not what was observed. This implies that the convection velocity of the eddy pattern varies much less rapidly with radius than the mean velocity.

As outlined in § 2.3, cross-correlations can be used to determine the convection velocity of the turbulence pattern U_c, and at the same time they define the autocorrelation of the turbulence in a frame moving with velocity U_c.

3.4. *Cross-correlations*

Cross-correlations were made of tape-recorded signals covering the mixing region of the jet as indicated by figure 3. A typical plot of the results for $M = 0{\cdot}45$ is given on figure 10. The results at $M = 0{\cdot}22$ are similar provided the time-axis is doubled. This indicates a strong Strouhal-number dependence in the turbulence signals. Each point on the space correlation representing a wire separation now becomes a curve on the $(R_{x\tau}, \tau)$-plane, where τ is the time delay on the signal from the upstream hot wire.

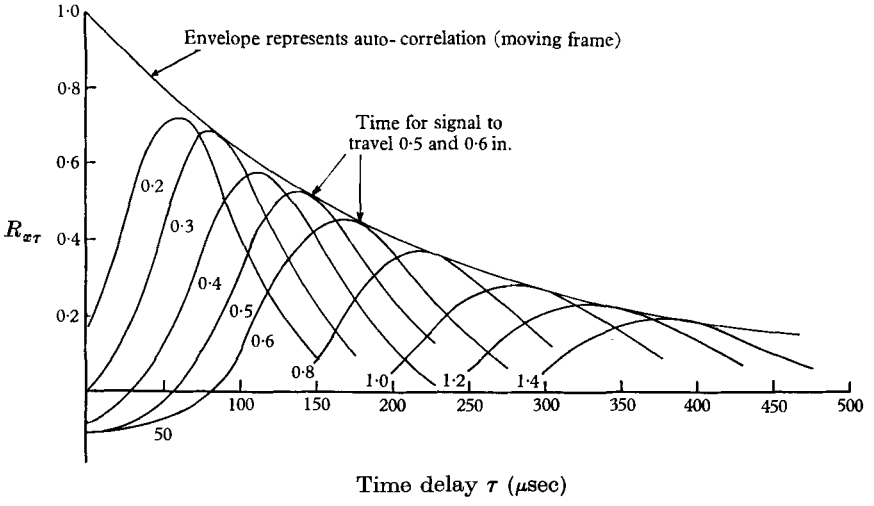

FIGURE 10. Cross correlation of axial velocity fluctuations with downstream wire separation. Numbers on curves represent separation (in.). $Y/D = 0{\cdot}5$, $X/D = 1{\cdot}5$ (fixed wire).

The envelope of these curves is the auto-correlation in a frame moving with the energy-containing eddies at the convection velocity U_c. The integral of the envelope is the moving-axis time-scale of the turbulence, while its Fourier transform is the spectrum function of the velocity fluctuations in a moving frame. This can be seen if one first considers the form figure 10 would take if the turbulence were a frozen pattern being swept past a stationary hot wire. Each curve representing a wire separation would rise to a peak value of unity, so the extent by which they fail to do so is a measure of the rate at which the velocity pattern changes. The time-scale is therefore related to the rate at which the velocity pattern is distorted, that is to the rate of generation of new turbulence.

Considering once more the turbulence in terms of vorticity, the generation of new turbulence is directly related to the rate at which the vortex filaments are stretched. It has already been demonstrated that the radial filaments are strongly stretched by the mean shear imply a continuous feed of energy into the axial and tangential velocity fluctuations. Furthermore, one would now expect to find a relation between the time-scale and the mean shear.

The moving axis auto-correlations $R_{\tau c}$ for a series of radial positions are plotted on figure 11 for two distances downstream from the orifice. They show that the

minimum time-scale corresponding to the maximum rate of generation of new turbulence is near the middle of the mixing region, where the shear is greatest. The relation between the integral time-scale and the inverse of the local shear $\partial x_2/\partial U$, which has the dimensions of time, can be seen best on figure 12. Included here are results obtained by Howard (1959) at 3 in. from the jet orifice and a result for $M_0 = 0{\cdot}22$. These results indicate that the integral time-scale is inversely

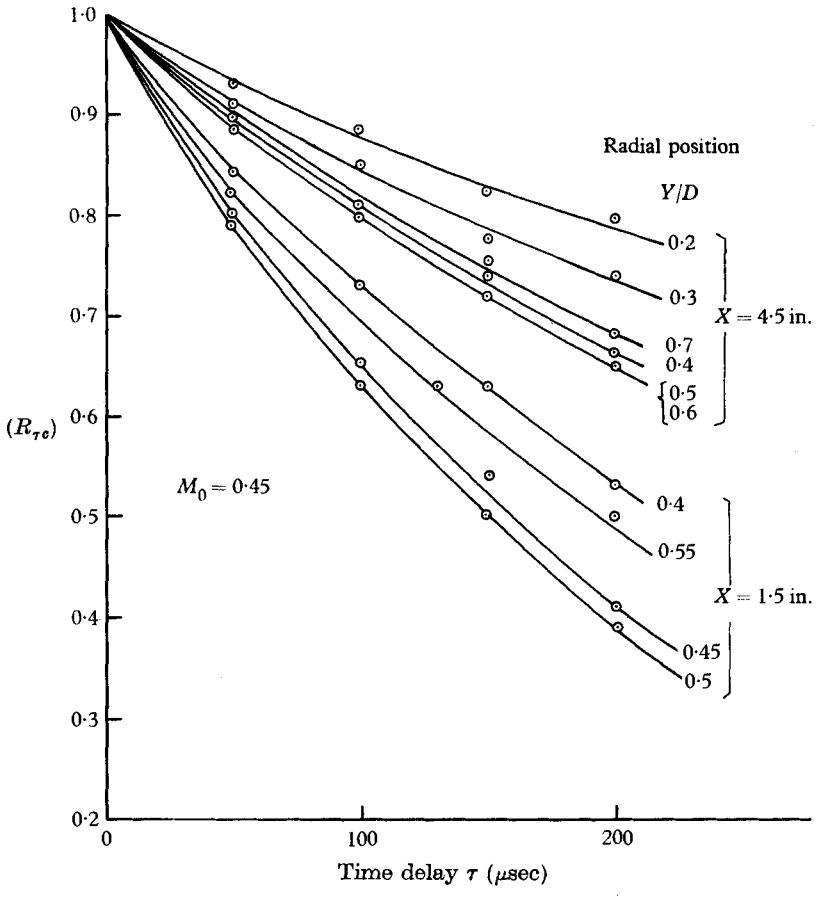

FIGURE 11. Moving-axis auto-correlations.

proportional to the local shear and suggest the local shear to be the time-scale parameter for similarity of turbulence time-scales and velocity fluctuations. The corresponding length scale is the distance from the orifice.

Equation (1.2) implies that in the absence of solid boundaries a frozen pattern of turbulence would generate little sound. The results on figure 12 show that the rate at which the velocity pattern is distorted is proportional to the shear. This fact with relation (2.9) implies that a relationship exists between the breadth of the moving-axis turbulent spectrum and the local shear.

Convection velocity. Returning to figure 10, the time delay at which each separation curve is tangent to the envelope will define a convection velocity U_c. Alternatively one could plot curves of constant time delay and variable separation

on the $(R_{x\tau}, x)$-plane. In this case each peak on the curves of constant τ gives a separation from which the convection velocity can be estimated.

Finally, the results can be plotted as isocorrelation contours on the (x, τ)-plane. This is shown in figure 13, where the upper diagram is equivalent to figure 10, and the slope of the broken line gives the convection velocity U_c. In the lower diagram the contours are replotted with respect to the broken line as an axis and now represent the isocorrelation contours in a frame moving at U_c. The radial distribution of convection velocity is plotted on figure 14. Here we see the

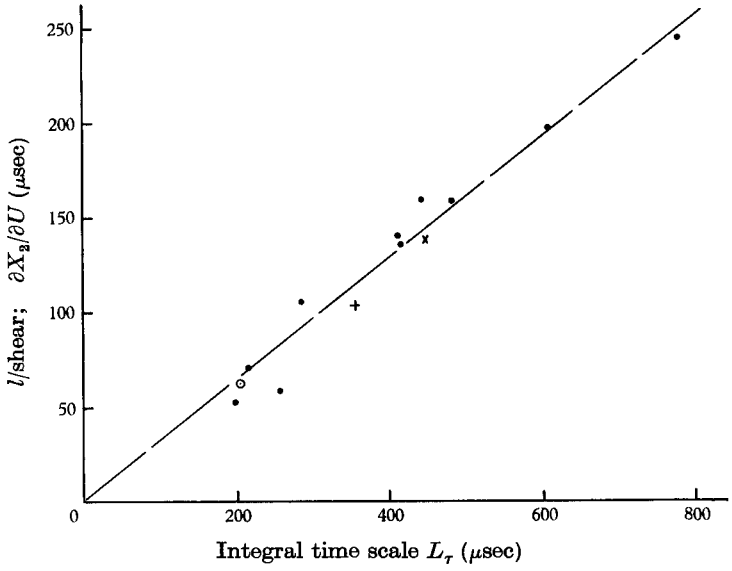

FIGURE 12. Variation of time-scale with local shear. +, $M_0 = 0{\cdot}34$, Howard; ●, $M_0 = 0{\cdot}45$ (figure 11); ⊙, $M_0 = 0{\cdot}45$; ×, $M_0 = 0{\cdot}22$ ($X = 1{\cdot}5$ in., $Y = 0{\cdot}5$ in.).

convection velocity approximates to the mean velocity for a limited region only, and does not exceed 0·7 of the jet velocity. Near the edge of the jet the convection velocity is several times the mean velocity. The radial gradient is not so steep as that of the mean velocity, even in the region of maximum shear. Thus, it seems reasonable to assume a constant convection velocity in the jet to simplify calculations of radiation patterns and frequency spectra.

Examination of the hot-wire signal with a cathode-ray oscilloscope provides an explanation of the difference between mean and convection velocity. This has been discussed by Richards (1959) elsewhere. Where the two profiles coincide, the signal appears symmetrical. At the edge of the uniform core of the jet the signal consists of random jumps representing short sudden drops in velocity well below that of the core. The change is large, of the order of $0{\cdot}5U_0$, and the signal appears as if it were made of two parts with different mean velocities. The faster moving part represents the steady core velocity U_0, with small velocity fluctuations superimposed on it, while the slower one consists of bursts of violent fluctuations superimposed on a lower mean value. In the outer part of the jet the inverse situation exists; here faster moving bursts of intense fluctuations

can be seen in a background of smaller fluctuations, which have a lower mean velocity. The more violent fluctuations, where they occur sufficiently frequently, will make a substantially greater contribution to the mean signal energy. The convection velocity will therefore be nearer to that of the large fluctuations, which contain most of the turbulent energy, than the mean velocity of the flow. That

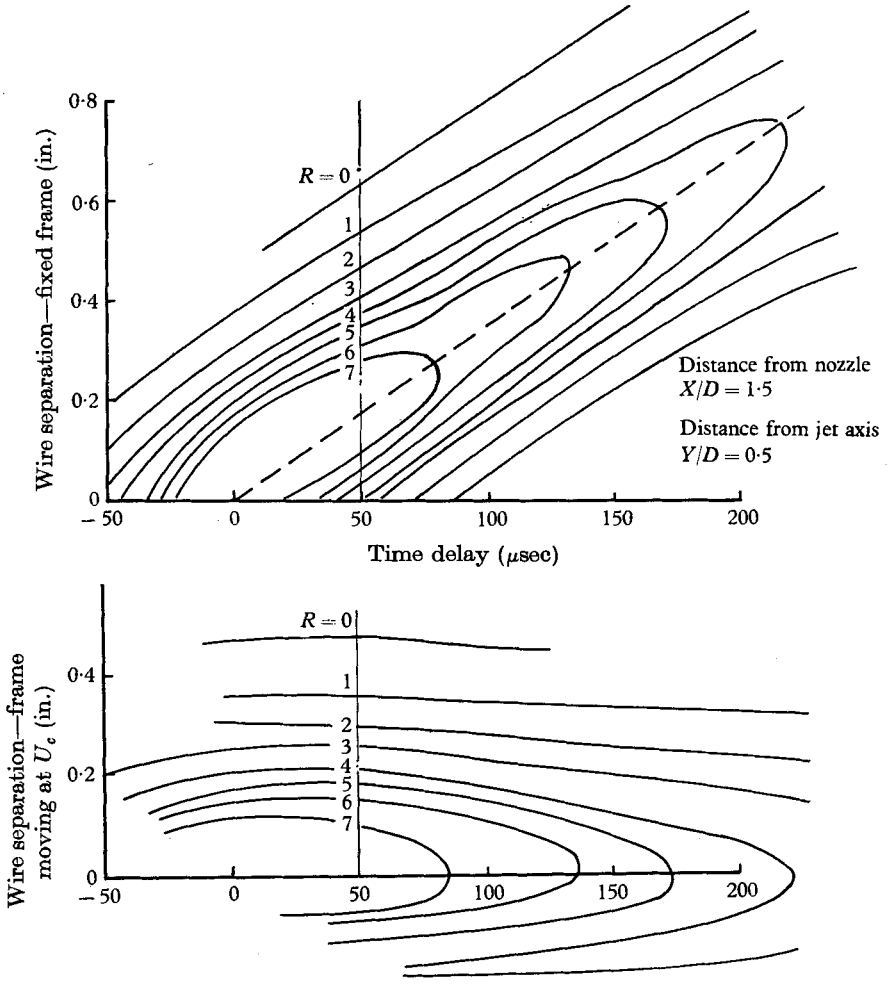

FIGURE 13. Isocorrelation contours of cross-correlations.

is, it will be lower than the mean velocity towards the core, and higher than the mean velocity at the edge of the jet. This distribution of convection velocity is consistent with the frequency spectra plotted on figure 9.

Ratio of time- to space-scales. The cross-correlations give the time-scale of the turbulence and its convection velocity U_c. The product of these quantities gives a length which is the distance a given pattern travels before it becomes significantly uncorrelated with its original form. The ratio of time-scale obtained this way to the length scale L'_x (equation (2.15)) is plotted on figure 15, which in-

dicates the way this ratio varies throughout the mixing region. These results are independent of the value of the jet velocity U_0, although the time-scales L_r' are not.

Apart from giving the general shape of the isocorrelation contours on figure 13, these results indicate that the regions of the jet where the turbulence may be

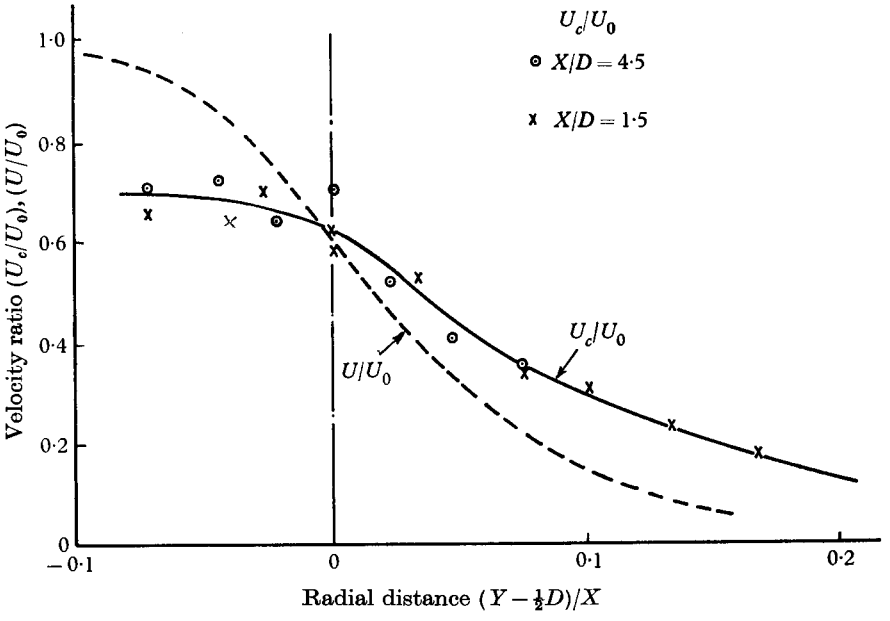

FIGURE 14. Radial distribution of convection velocity.

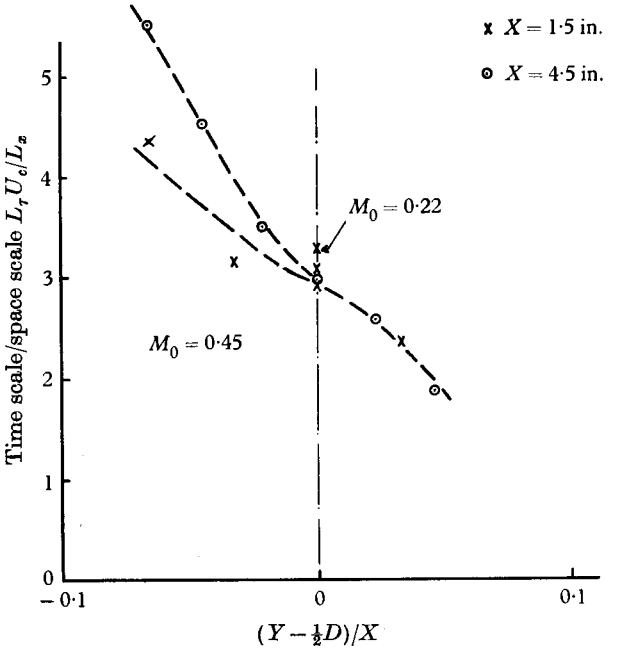

FIGURE 15. Ratio of time- to space-scales for axial velocity fluctuations.

regarded as a frozen pattern convected at U_c are limited. They also show that it can be misleading to obtain the space-scales by transforming the fixed-point auto-correlations or spectra with the local mean velocity. This explains why the space-scales Laurence obtained by this method (figure 30 of his paper) decrease rapidly radially outwards, while those obtained by integrating his two-wire correlation curves do not.

Finally, the results indicate in a general way the relative magnitude of the first time-derivative of T_{ij}. Similarly they indicate even more roughly the way in which the magnitude of the integral in equation (1.2) varies. This suggests that a given volume of turbulence will generate relatively more noise as the ratio of time- to space-scales decreases, since this indicates that the turbulent pattern is changing more rapidly.

3.5. *Turbulent intensity measurements*

The intensity of the axial velocity fluctuations was determined from the linearized hot-wire signal with a Dawe true R.M.S. meter. This instrument is specially designed to cope with signals that have a large ratio of peak signal to R.M.S. values.

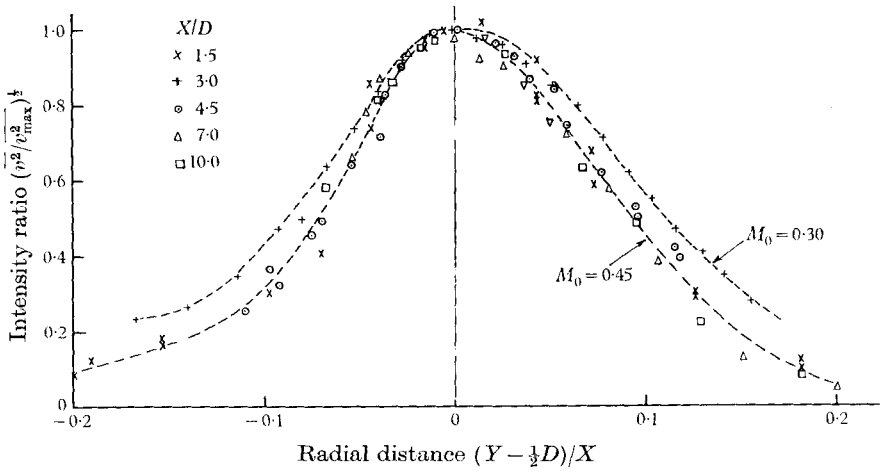

FIGURE 16. Comparison of radial distributions of axial turbulent intensity.

This is essential, bearing in mind the form of the hot-wire signal described in § 3.4 above. For the same reason it is probably more desirable to employ a linearized hot-wire anemometer for the measurements, since the measured intensity will depend on the slope of the velocity bridge-voltage calibration curve, which varies with the mean velocity.

The radial distribution of turbulent intensity in the shear layer is best seen in figure 16 where the results have been plotted on a dimensionless basis. To aid comparison the intensity has been divided by the maximum intensity, and the results for various axial distances can then be compared directly. There is a considerable scatter in the results but a general tendency for the distribution to become more peaked as the Mach number increases seems to be well defined. The dependence of the turbulent intensity distribution on Mach number is

also shown on figure 17. Here the peak intensity has been plotted for two Mach numbers, and it can be seen that the intensity rises more rapidly near the orifice at the lower Mach number.

The size of the mixing region is related to the length-scale L_x while the time-scale is related to the local shear $\partial U/\partial x_2$. The product of these two quantities has the dimensions of a velocity termed hereafter the shear velocity U_s, where $U_s = L_{x_1}\partial u/\partial x_2$. Since the rate of generation of new turbulence is proportional

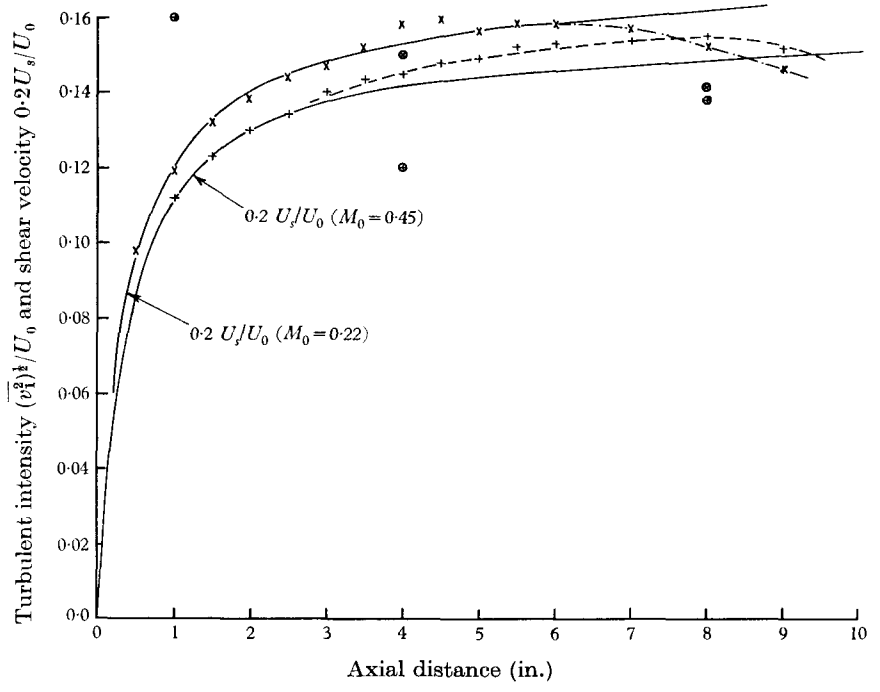

FIGURE 17. Axial distribution of peak turbulent intensity. Laurence: ⊕, $M_0 = 0{\cdot}5$; ⊗, $M_0 = 0{\cdot}3$. Peak intensity: ×, $M_0 = 0{\cdot}20$; +, $M_0 = 0{\cdot}45$.

to the shear, it seems likely that a relation exists between the turbulent intensity and the shear velocity, which proves to be the case. The mean shear is shown on figure 6 for $M_0 = 0{\cdot}45$, while the corresponding length-scale is given on figure 8, and thus the axial distribution of shear velocity can be calculated. This has also been plotted on figure 17, where it can be seen that $0{\cdot}2U_s$ is equal to the intensity to a fair approximation. The curve for $M_0 = 0{\cdot}22$ was obtained from two determinations of the maximum shear and then making the assumption that the maximum shear distribution had the same origin as the results on figure 6. This relation between turbulent intensity and shear velocity is also supported by the results on figure 18, where the radial distribution of shear velocity—estimated from the results on figure 5 with length-scales obtained by interpolation from figure 7—has been plotted together with the observations of the intensity. Again the agreement is good leading to the relation $(\overline{v_1^2})^{\frac{1}{2}}/U_0 = 0{\cdot}2U_s/U_0$.

Laurence also obtained intensity measurements in the same region of the jet and, although somewhat more scattered, they are of the same order of magnitude

as shown on figure 17. At 14 in. from the orifice his intensity measurements indicate values between 0·14 and 0·15 which agree with results not shown on figure 17. His measurements also confirm the decrease of intensity with increase of Mach number for the first few diameters downstream from the jet orifice. This implies a decrease in the local shear with increase of Mach number in the region where the potential core exists. This seems to be indicated by the present results as mentioned earlier, but further experiments are required to confirm this relationship.

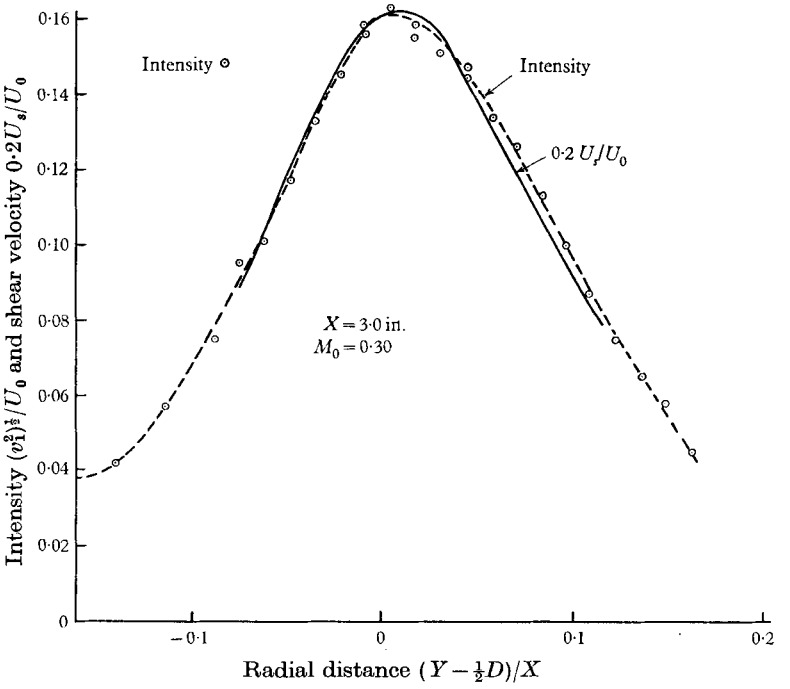

FIGURE 18. Radial distribution of turbulent intensity.

4. Discussion of results

Before examining the results it is profitable to reconsider the probable sources of major errors. Both the linear and non-linear wire signals include a small proportion of the radial and tangential fluctuations. This will have a significant effect near the outer edge of the jet, where the mean velocity is small and the local fluctuations of velocity are relatively large. This will introduce errors in both the intensity measurements and in the correlations in this region of the flow. There seems little to choose between the linear and the non-linear hot-wire sets in this regard, as is shown in § 2.2. The latter requires more careful calibration, but this is offset somewhat by the smaller contribution from the radial and tangential intensities. Flow reversal for which there is some evidence in the readings near the edge of the jet will also cause errors in the measurements. A further source of error is to be found in the problem raised by the form of the signals themselves. They often have peak levels six to eight times the R.M.S. level, which means they must be recorded at low R.M.S. signal levels to avoid clipping or

distorting the signal. This places severe limitations on the acceptable noise levels of the recording equipment, which is most serious in the correlations. If the noise-to-signal ratio is q (mean square values) on both channels, then the ratio of the correlation coefficient to that in the absence of noise is $1/(1+q)$.

The general agreement with the measurements made by Laurence and others is good in regions of the flow where fair accuracy can be expected. The present results are more detailed than those of Laurence in the regions of high shear. His results on the other hand extend over a much larger portion of the flow. For this reason the two sets of results are complementary and provide data for a wider range of conditions than each set alone. This has been useful in obtaining similarity relations to describe the turbulence.

4.1. *Similarity relations for jet turbulence*

The general similarity of the mean velocity profiles of the jet has been well established for some time. The geometry of the potential core and the mixing region is similar for all subsonic cold jets and is illustrated in figure 3. It has been well established that the jet diameter is the scale parameter for similarity of jet geometry.

Length scales. The axial scale of the turbulence defined by the correlation measurements was found during the experiment to be fitted by the expression

$$L_{x_1} = 0{\cdot}13X \quad (D < X < 6D). \tag{4.1}$$

This expression implies a zero scale at the jet orifice which is not really plausible physically. However, it is very difficult to make measurements close to the jet orifice, and the scale here will be influenced by the boundary layer in the nozzle. As this is very thin it was assumed that the scale could be regarded as negligible.

Laurence found the radial scale was about one-third of the longitudinal scale L_{x_1} for the first few jet diameters and so also did Townsend (1956) for $X/D > 20$. Experiments are in hand to confirm this and to measure the tangential scales. As argued above it is anticipated the tangential scale will be similar to the axial scale.

Reference to figure 7 shows that the length-scale L_{x_1} varies slowly as one moves radially across the mixing region having a minimum at the point of maximum shear. This is in agreement with the measurements that Laurence made of two-wire correlations. The scales he obtained by transforming the spectra decrease rapidly towards the edge of the jet from a maximum at the point of maximum shear. This can be explained by his use of the mean velocity for the transformation which is lower than the convection velocity. When the convection velocity is used for the transformation the length-scales become more constant.

Time-scales. The moving-axis time-scales were also found to be almost constant radially across the middle of the mixing region (figure 11) and to increase axially along the jet. The time-scale was also found to vary almost exactly as $1/U_0$. This can all be explained in terms of the local shear, if it is assumed that the time-scale is inversely proportional the local shear. The results on figure 6 show that the shear varies almost directly as the jet velocity, while those on figure 5 show it is substantially constant across the middle of the mixing region. The assumption is supported by the results plotted on figure 12, where the time-scale L'_τ defined

by equation (2.14) is plotted against the inverse local shear. A fair fit to the points is given by the relation

$$L_7' \simeq 3/(\partial U/\partial x_2), \tag{4.2}$$

and this relation suggests that the inverse of the local shear is a good time-scale parameter for defining similarity of kinematic properties of the jet flow. The local shear was found to be expressed by

$$\partial U/\partial x_2 = 6U_0/(X + ka_0)\,\mathrm{sec}^{-1} \quad (M_0 = 0{\cdot}45), \tag{4.3}$$

where ka_0 has the value 0·4 in. for the 1 in. jet used at Southampton. It seems reasonable to assume that k depends on the boundary layer at the lip of the jet. This implies that a similar small constant is missing from equation (4.1).

4.2. *Turbulence intensity*

Intensity measurements were difficult to make accurately since their interpretation depends on the local slope of the voltage–velocity calibration curve. For the linear set the variation of the slope of the straight line was measured carefully and was found to be constant within 5 % at all except very low velocities, where the variation was 10 %. Provided they were set to standard conditions all wires gave the same linearity performance. During the experiments it was found that occasionally the resistance of the wire changed suddenly by as much as 10 %. This generally occurred during a high-speed run and there is good evidence it was due to mechanical damage which was not severe enough to break the wire. After such a change the calibration remained stable once more. Such occurrences were easy to detect provided simple rechecks were included in the experiments. With a non-linear wire it was much more difficult to make accurate intensity measurements, as it was often necessary to recalibrate the wire after each run.

The correlations remain unaffected by such changes, since the magnitude of the electrical signal does not appear in the relation for the correlation coefficient. The small changes in slope do not affect the accuracy of the mean velocity measurement, but the sudden changes of resistance do. The effect is less serious here as it is always immediately obvious when the results are plotted if not before. This may explain the scatter of Laurence's results plotted on figure 17, as they were made with non-linear equipment. In the present experiments the intensity measurements from runs where such difficulty occurred were discarded and the measurements repeated.

The conclusion from the results in figures 17 and 18 is that the intensity appears to be proportional to the shear velocity. This is expressed by the relation

$$(\overline{v_1^2})^{\frac{1}{2}} = 0{\cdot}2L_{x_1}(\partial U/\partial x_2). \tag{4.4}$$

Alternatively, if the local shear is proportional to the Mach number then the relation (4.4) would become

$$(\overline{v_1^2})^{\frac{1}{2}} = 0{\cdot}2KL_{x_1}(\partial U/\partial x_2), \tag{4.4a}$$

where K is approximately unity but decreases slowly with increase in the jet Mach number. We can substitute for L_{x_1} from (4.1), and from (4.3) for the shear $\partial U/\partial x_2$ in (4.4) to give the maximum value of the intensity in the mixing region

$$(\overline{v_1^2})^{\frac{1}{2}}_{\max} = 0{\cdot}2(0{\cdot}13X)\,[6U_0/(X + ka_0)] \quad (M_0 = 0{\cdot}45),$$

and when X is large, say $10ka_0$,

$$[(\overline{v_1^2})^{\frac{1}{2}}/U_0]_{\max} \simeq 0{\cdot}16. \tag{4.5}$$

This agrees well with all the published measurements in a jet. (See Townsend 1956, Corrsin & Uberoi 1951.)

The change in maximum intensity with jet Mach number is not included in this analysis unless the shear varies with Mach number. Although it appears to do so, the way in which it does vary it not yet established with any certainty.

Combining (4.2) and (4.4) leads to the relation

$$(\overline{v_1^2})^{\frac{1}{2}} L_r'/L_{x_1} = 0{\cdot}6, \tag{4.6}$$

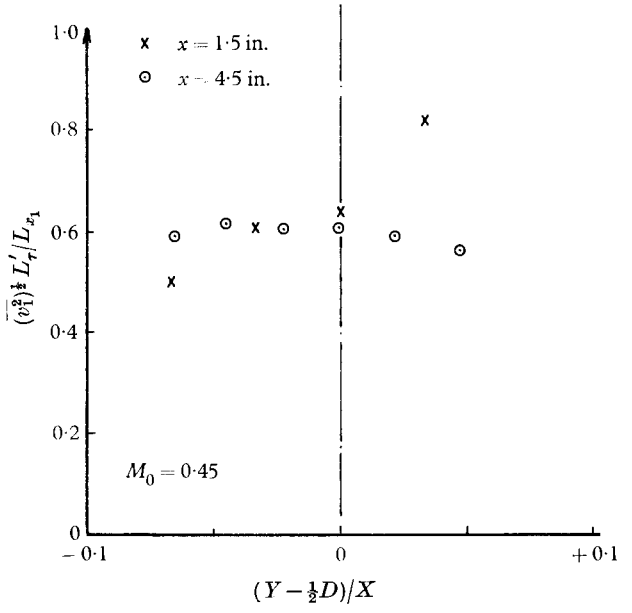

FIGURE 19. Ratio of time-scale times intensity to length-scale for axial velocity fluctuations.

which should also be satisfied by the measurements. This provides an independent check of each of the ratio of time-scale to space-scale measurements plotted on figure 15. The results on figure 12 have therefore been replotted on figure 19 according to equation (4.6). It can be seen that the agreement is good at 4·5 in. downstream but rather more scatter exists for the results obtained 1·5 in. downstream, particularly near the edge of the mixing region. This is more or less to be expected when one considers that a small error in the position of the hot wires becomes relatively more serious as one approaches the jet orifice. Examination of the results on figure 12 also illustrates this argument with respect to relative scatter since the time-scale decreases as one approaches the jet orifice.

4.3. *Turbulence spectra*

The spectra of the turbulence in a frame moving with the turbulence can be found by transforming the moving-frame auto-correlations such as are shown on figure 10. These, in their turn, have the same shape for the first four or five jet diameters,

while their scale is inversely proportional to the local shear and can be found from equation (4.2). Thus, the spectral density distribution of the turbulence can be estimated once the shear distribution in the jet is known.

The axial distribution of the shear $\bar{e}_{12}$ is given by equation (4.3), while the radial distribution may be found from figure 5. Since the shear and intensity all vary slowly near the region of maximum intensity, the jet turbulence spectrum may be approximated by that in the middle of the mixing region.

A further simplification is possible since it was found (figure 14) that the convection velocity of the turbulence varied slowly here and was equal to $0{\cdot}6U_0$. The fixed-wire auto-correlations and the moving-frame auto-correlations are directly related through the convection velocity. The space-scale can also be found by using this velocity to transform the fixed-wire auto-correlations as indicated by Laurence. He found good agreement between measured and estimated scales in the centre of the mixing region where the convection velocity approximates to the local mean velocity. The validity of this process is confirmed by the results on figure 15, which shows that the turbulence is well represented by a frozen pattern convected past a fixed point at the velocity U_c, since the time-scale $U_c L'_\tau$ is large compared with the space-scale L'_x.

4.4. *Estimation of effective source strength*

The similarity relations describing the length-scales, shear and intensity can be inserted into Lilley's expression (equation (1.6)), for the intensity per unit volume. For present purposes this involves estimating the quantity $L_{x_1}^5(\partial U/\partial x_2)^6 \overline{v_1^2}$ and ignoring the variation in $\overline{\rho^2}$ which was not measured. This is shown plotted on figure 20 as contours on a radial plane with a distorted radial scale. The high-intensity areas are quite small, and extend mainly over the regions of approximately constant shear. Close to the jet lip the higher shear is balanced by the low intensity and length-scales, while more than five diameters downstream, the fall in shear more than balances the increases in the length-scales. Beyond this point there is good evidence by Laurence (1956) and others (Townsend 1956) that the length-scale increases more slowly when the potential core has vanished. This will reduce the intensity along the axis of the jet more rapidly beyond the first five or so diameters than the similarity relations suggest. This tendency is indicated by the results in figure 17. It is worth emphasizing that the contours on figure 19 refer to the 1 in. jet and should be considered in terms of the expressions from which they were calculated. For example, a small change in the expression for length-scale would change the distribution close to the jet orifice considerably. Similarly, in a larger jet, the contours would represent the source strength distribution close to the jet orifice only.

4.5. *Turbulent structure of the mixing layer*

The experiments give some insight into the physical structure of the turbulence in the mixing region. The results show that there is an initial zone in which the turbulence intensity grows rapidly. The extent of this is only a few inches and depends on the dimensions of the boundary-layer flow at the jet orifice. Beyond this there is a region extending well past the end of the potential cone where the

intensity is constant, and the flow is in equilibrium. Townsend (1956) shows that the flow is self-preserving and may be represented by a single family of equations from 8 to 20 diameters from the jet orifice. The present results indicate that a further self-preserving region extends from eight or so diameters to close to the jet orifice, but further experiments are required to extend the similarity relations for jet turbulence given above to regions beyond the first eight or so diameters.

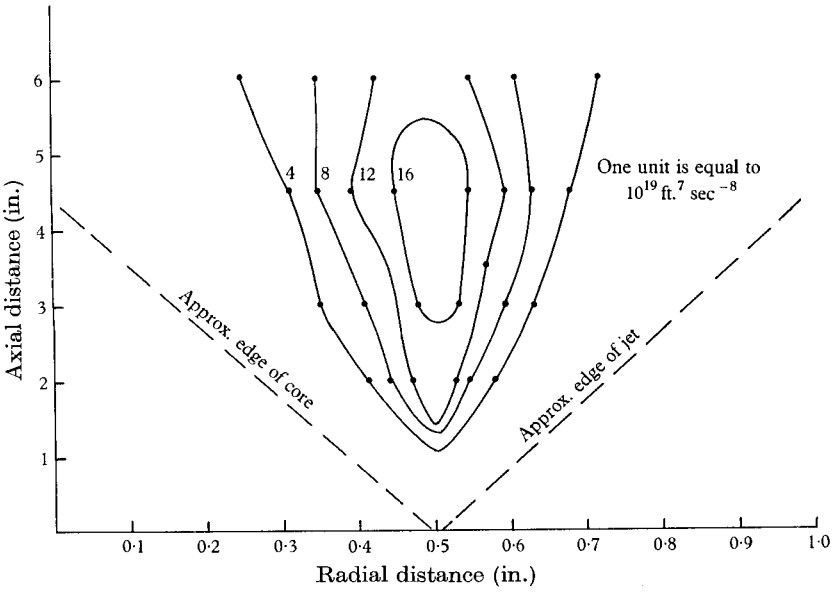

FIGURE 20. Distribution of source strength in a 1 in. jet.

The mixing-region flow consists of a system of eddies which originate near the jet orifice and grow steadily as they travel down the jet. The growth of the eddies is dominated by the local mean shear which has a strong influence on the eddy shape and the distribution of the velocity fluctuations within the eddy. The shape of the eddies themselves is also indicated by the results. The feed of energy into rotations about radial axes suggests that they are flattened in the radial direction and are therefore somewhat disk shaped. The radial distribution of axial intensity is shown on figure 18, and using this model of the turbulence structure one can speculate on the probable form of the radial distribution of radial turbulent fluctuations. Since the flow is axially symmetric, contributions to the radial fluctuations must come from stretching of axial vorticity filaments. There is also a mean shear in the axial direction, which is largest at the inner edge of the mixing region, or on the jet axis beyond the end of the potential core. This suggests that the radial intensity decreases as one moves radially outwards across the mixing region, and some measurements by Corrsin (1943) seem to support this conclusion.

The radial distribution of tangential velocity fluctuations will be similar to the distribution of axial fluctuations, modified by an extra but smaller contribution from the stretching of the axial filaments particularly at the inner edge of the mixing region.

Finally, these arguments suggest an alternative form of equation (4.4), it being more reasonable to suppose the radial scale of the axial fluctuations L_{x_2} to be more closely related to the axial turbulent intensity than the axial scale. This relation then becomes, for the middle of the mixing zone,

$$(\overline{v_1^2})^{\frac{1}{2}}_{\max} = \tfrac{2}{3} L_{x_2} (\partial U / \partial x_2)_{\max}, \tag{4.7}$$

but further measurements on the distribution of L_{x_2} are required before this relation can be applied throughout the mixing region.

4.6. *Conclusions*

The turbulence measurements have shown that there are well-defined similarity relationships for the first six or eight diameters of the jet flow, as well as those already known for further downstream. These break down close to the jet orifice where the shear layer is very thin. Kinematic similarity can be established for intensity, space-scales, time-scales and spectra in terms of the distance from the jet orifice X, and a local time-scale which is most suitably expressed in terms of the inverse of the local shear.

There is some uncertainty concerning the magnitudes of the space-scales over the first ten diameters, and this requires further investigation. More measurements of the radial distribution of convection velocity are required and a careful study of the variation of local shear and intensity with Mach number. The application of the similarity laws to distances beyond six diameters needs studying as it is anticipated that substantial differences will be found once the potential core vanishes.

The results confirm the conclusions of previous investigators and in addition it has been shown that the statistical characteristics of the turbulence can be expressed fairly accurately by simple relationships.

The authors wish to thank Professor E. J. Richards and other members of the department for the many helpful suggestions offered during the course of the work. Thanks are also due to D.S.I.R. and to the Ministry of Aviation for financial support and their interest in the investigation and finally to Dr N. Curle for editorial suggestions in writing this paper.

REFERENCES

ALLCOCK, G. A., TANNER, P. L. & MCLACHLAN, K. R. 1962 A general purpose alanogue correlator for the analysis of random noise signals. *Univ. Southampton Aero. Astr. Rep.* 205.

CORRSIN, S. 1943 Investigation of the flow in an axially symmetric heated jet of air. *NASA, War-time Rep.* no. W. 94.

CORRSIN, S. & UBEROI, M. S. 1951 Spectra and diffusion in a round turbulent jet. *NASA Rep.* no. 1040.

CURLE, N. 1961 The generation of sound by aerodynamic means. *J. Roy. Aero. Soc.* **65**, 724.

DAVIES, P. O. A. L. 1957 The behaviour of a Pitot tube in transverse shear. *J. Fluid Mech.* **3**, 441.

GERRARD, J. H. 1956 An investigation of the noise produced by a subsonic air jet. *J. Aero. Sci.* **23**, 855–66.

HOWARD, J. B. 1959 An investigation into the applicability of Taylor's hypothesis in an open jet of air. Honours Thesis, Univ. Southampton (unpublished).

LAURENCE, J. C. 1956 Intensity, scale and spectra of turbulence in mixing region of free subsonic jet. *NACA Rep.* no. 1292.

LIGHTHILL, M. J. 1952 On sound generated aerodynamically. I. General theory. *Proc. Roy. Soc.* A, **211**, 564–87.

LIGHTHILL, M. J. 1954 On sound generated aerodynamically. II. Turbulence as a source of sound. *Proc. Roy. Soc.* A, **222**, 1–32.

LIGHTHILL, M. J. 1962 Sound generated aerodynamically. The Bakerian Lecture, 1961. *R.A.E. Tech. Mem.* no. DIR 8.

LILLEY, G. M. 1958 On the noise from air jets. *Aero. Res. Counc., Lond.*, 20,376-N. 40-F.M. 2724.

LILLEY, G. M. & WESTLEY, R. 1952 An investigation of the noise field from a small jet and methods for its reduction. *College of Aeronautics Rep.* no. 53.

PROUDMAN, J. 1952 The generation of noise by isotropic turbulence. *Proc. Roy. Soc.* A, **214**, 119.

RIBNER, H. S. 1958 On the strength distribution of noise sources along a jet. *Univ. Toronto, Inst. Aerophys. Rep.* no. 51.

RICHARDS, E. J. 1959 Recent developments in jet noise research. *Proc. 3rd Int. Congr. on Acoustics.*

SANDBORN, V. A. & LAURENCE, J. C. 1955 Heat loss from yawed wires at subsonic Mach numbers. *NACA TN*, no. 3563.

TAYLOR, G. I. 1935 The statistical theory of turbulence. I. *Proc. Roy. Soc.* A, **151**, 421.

TOWNSEND, A. A. 1956 *The structure of turbulent shear flow*, ch. 8. Cambridge University Press.

WEBSTER, C. A. G. 1962 A note on the sensitivity to yaw of a hot-wire anemometer. *J. Fluid Mech.* **13**, 307.

WILLIAMS, J. E. FF. 1961 The noise from turbulence convected at high speed. *Aero. Res. Counc., Lond.*, 23,323-F.M. 3138-N. 184.